Section A-Research paper
ISSN 2063-5346

Development and Analysis of Rolling Contact Fatigue Squat Crack in Wheel/Rail-Weld System Using Finite Element Modelling

Mahesh Bhiwapurkar[1,a*] Prakash Kumar Sen[2,b], and S.P. Harsha[3,c]

[2]Professor, Mechanical Engineering Department, O.P. Jindal University Raigarh, India

[1]Research Scholar, Mechanical Engineering Department, O.P. Jindal University Raigarh, India

[3]Professor, Department of Mechanical & Industrial Engineering, IIT Roorkee, India

*mahesh.bhiwapurkar@opju.ac.in, prakashkumarsen@gmail.com, surajfme@iitr.ac.in

---

Keywords: Alumino thermite rail-weldment, Finite element method (FEM), ANSYS, Rolling contact fatigue (RCF), Squat, Multi-axial fatigue.

Abstract. One of the leading issues facing the railway sector is the occurrence of rolling contact fatigue fractures on the surfaces of the rail, its weld, and wheels. In the present study, a FEM model was investigated on an Aluminium-Thermite weld to estimate the beginning of fatigue cracks. The investigated model comprises a FEM analysis that accounts for the material behaviour due to the contact pressure between the rail weldment and the running wheel. The rail with its weldment and the wheel is modelled using FEM in ANSYS space-claim with a squat type of semi-elliptical crack. Force is applied vertically on the wheel's axle, then rolled on the rail weld assembly in the longitudinal direction. The resulting stress and strain values for the critical plane were integrated with the life calculation model under multi-axial fatigue to estimate the beginning of fatigue cracks. The study also estimates fatigue damage parameters at the contact region. To initiate the crack initiation, a fracture length of 0.5 mm on the curve of the weld was considered, and the cycle calculation was obtained. The maximum contact pressure is estimated to be approximately 2×10^6 cycles. The study involves two sub-models for analysis with different boundary conditions, revealing the numerical prediction of initiation of 0.5 mm-long cracks with cycle counts as 7.47×10^6 cycles for Model-I and 3.87×10^6 cycles for Model-II. Results are validated with other literature findings and proposed modifications.

Introduction

One of the common issues in the railroad sector is RCF damage on wheels, rails, and their weld's running surfaces. Two forms of surface-initiated cracks found in rails and their welds are head checks and squats. During curvilinear motion at the contact of the wheel and the rail weld, initially, head checks formation starts on the gauge corner side to the new rail. These tiny, shallow-angled

fissures are pretty uncertain. Head checks move in the same direction as the material's microstructure that the vehicle's pulling force has distorted. Squats are fissures that develop on rail or weld crown surfaces. It begins as tiny fissures and progresses toward the rail crown at a little inclination concerning its upper surface. Once it reaches a definite length, it begins to develop in branched cracks, which, if allowed to continue, will result in catastrophic failure. These fissures typically appear on rails, transporting fast trains and cargo yearly. For railroad firms worldwide, it poses a particularly critical issue. The amount of time rail maintenance operators need to grind the rails' surface to remove RCF cracks and other defects is decreasing due to heavy traffic. It has been hypothesized that eliminating such cracks before they deepen may require grinding in squat-prone places to prevent the rail weld's failure [1]. This grinding technique includes issues to note the period between subsequent repairs of rail or weld cracks for maintenance records.

To study the head check defect and squat crack in rail wheels, fatigue analysis has been performed using the critical plane approach for low-cycle fatigue and ratcheting strain accumulation [2]. Tensor analysis for stress and strain has also been conducted to identify the most damaging plane [3]. The study on squats cracks involves analyzing the co-planar crack growth phenomenon [4]. Overall, extensive FEM analysis has examined various defects in rail wheels.

Numerical modelling for the start of squat cracks has been built in the present paper for achieving a goal to forecast the location, flow of cracks, and fatigue crack initiation cycle. To replicate low-cycle fatigue behaviour with a decreasing rate of material hardening, the model used in this study uses a combined isotropic and kinematic hardening rule. The fracture start is then predicted using conditions related to the response of materials under cyclic load based on findings by Li et al. [20]. ANSYS is used for all modelling and simulations carried out.

Rail welds and their damage formation

The derailment of a train may be caused by a fractured rail or weld. The rail weld exhibits a geometric irregularity for damage formation compared to plain rail. The weld results in a geometric irregularity at the contact surface of wheel motion, causing dynamic fluctuations in axle load with amplification in contact stress. Normal and creep stresses develop with their dispersal within the surface contact area. Another factor contributing to this phenomenon is the existence of material inconsistencies present on the surface of the wheel or rail. These factors encompass non-uniform rigidity sharing on the rail contact surface, micro-structural perturbations, specific nonmetal insertions, or inequalities in steel phases on or beneath the surface. Another contributing factor to this phenomenon is core material inhomogeneity or knots within the weld. The micro cleanliness of the weld metal in its casting state is typically lower quality than the parent material. Typically, the

said mechanisms do not operate in isolation when contributing to harm; rather, it interrelates, substantially accelerating the spread of pre-existing damage.

The preceding information indicates that the Alumino-Thermic weld is prone to these occurrences. Geometric abnormality observed at rail weld, which is prevalent in most cases, may be attributed to a significant material defect (deficiency in fusion or porosity). In a weld, premature failure may occur during cold winter conditions when high tensile forces are exerted on the rail [5,6]. Hence, it can be inferred that inside material or blended defects are typically not accountable for enduring degradation on the mating surface of the wheel and rail. The non-uniformity of the rail surface can cause localized variations in contact stresses during rolling contact. This results in disparate shakedown in material, work hardening property of weld surface, and plastic deformation along its length [7]. This phenomenon can also lead to non-uniform wear, surface cracking, and gradual geometry degrading of the rails and welds. The procedure mentioned above is commonly referred to as weld batter, as noted by Mutton and Alvarez [8]. Illustrations of this occurrence are depicted in Figure 1. A specific type of damage initiated at the surface by RCF is known as a squat fault. Rail welds are frequently observed as initiators of corrugation or squat-type defects [9,10,11].

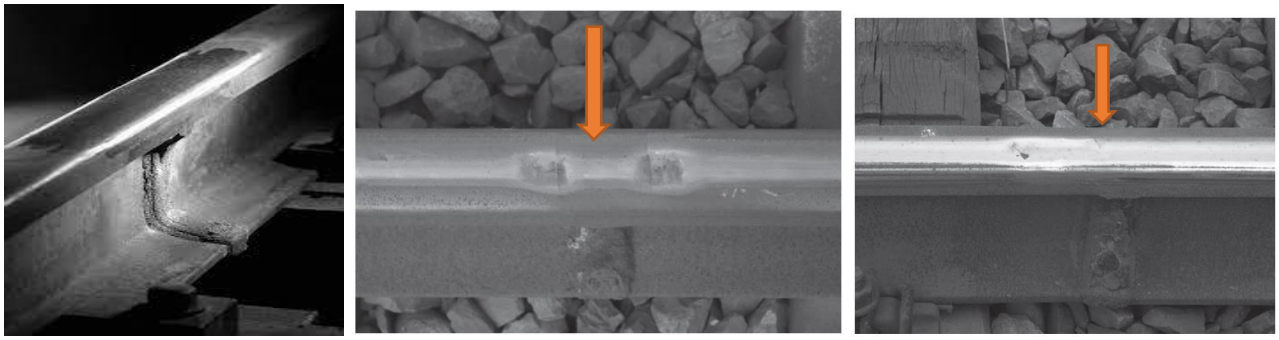

(a) (b) (c)

Figure 1 (a) AT-weld in rail (b) squat generation on AT weld (c) Growth of crack

Horizontal splitting may occur on web areas due to fatigue, resulting in heavy freight carrying tracks for both curved and straight tracks and characterized as low cycle fatigue under heavy axle load with fast fracture propagation on the collar at weld due to slag-induced imperfection [8].

Squats at rails and their weldments

A squat is identified as a shallow indentation located approximately at the midpoint of the rail or weld head on both straight and slightly curved tracks. The observed depression is attributed to subsurface cracking, diminished material strength, and accumulation of debris within the affected area, resulting in a visually distinct darkened region. Figure 2 (a) illustrates instances of squats executed on alumino-thermic welds.

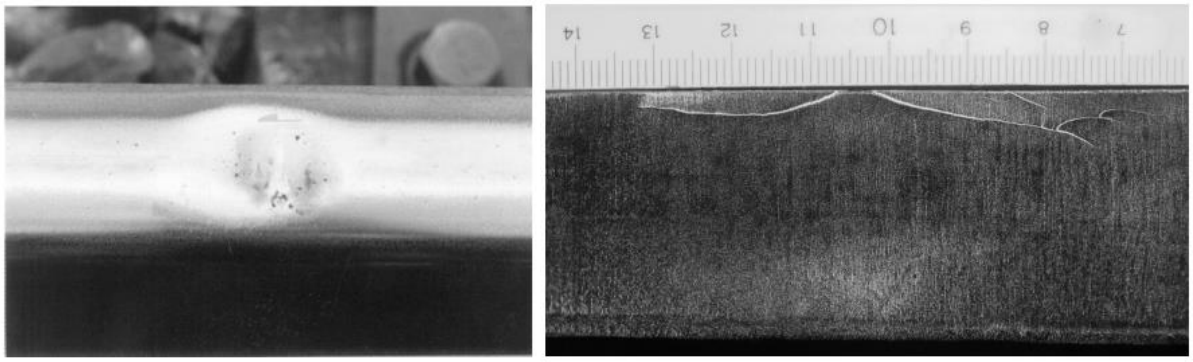

a) Squat on rail surface b) Short leading and long trailing crack on rail cross-section

Figure 2 (a) Squat represented as a dark spot on rail surface (b) Two primary initiated cracks in leading and trailing direction revealed in RTRI, JAPAN [14].

Examination of the squat's cross-section reveals the presence of two cracks. One of these cracks is a short primary crack spreading toward wheel motion. At the same time, the other is quite longer trailing crack that propagates at an angle, approximately 30° with a horizontal plane, shown in Figure 2(b). The trailing crack experiences a higher stress concentration at its tip than the leading crack in driving wheels [12,13]. As a result, the trailing crack's growth rate is higher and tends to become longer in regions with high tractive effort. The occurrence of multiple minor branch cracks emerging from a trailing crack is a common phenomenon whereby one of these cracks may propagate down towards the rail head and instigate a transverse fracture.

The martensite (phase of steel), which is fragile, is prone to cracking and triggers a surface crack that subsequently spreads due to the rolling contact forces. This results in the formation of trailing cracks which is characteristic of squats [14]. High tractive effort significantly contributes to extreme surface shear for initiating RCF cracks [15]. These results to surface cracks which convert into leading and trailing directional cracks as shown in Figure 2. (b). Regular grinding can treat these issues, which removes a thin layer of metal from the rail or weld head surface on the most deteriorated area, and the crack initiates first. The Shinkansen model has been shown to respond well to frequent preventive grinding [16].

Li et al. [21] discovered squats' size under dynamic contact between rail wheel systems. They provided a comprehensive overview of recent progress in research on rail wheel contact and welds in a review article. The study also highlighted significant developments in understanding the mechanism of RCF failure and identifying key factors that affect the RCF life cycle. Various approaches to mitigating RCF failures, including material selection, surface preparation, and structural design, were also discussed [17,24]

Analysis of Squat Defects

Initial crack growth occurs at a narrow angle with the rail head surface. The narrow-angle crack tends to turn toward the transverse plane when it is 3 to 5 millimeters deep.

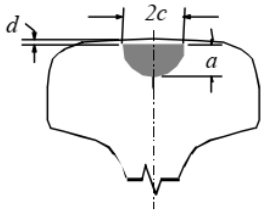

Figure 3 Squat Type of defect in a rail section

Figure 3 depicts an idealized version of the defect named 'squat'. The term aspect ratio as per dimension in the above figure is defined as 'a/c'. The ultrasonic test results show that the squat defect's aspect ratio is roughly 1, considered a surface fault with either semi-elliptical or semi-circular shapes [18].

The SIF for a semi-elliptical surface defect is determined [18] by

$$K_I = 1.12 M_1 \sigma \frac{\sqrt{\pi a}}{E(k)} \qquad \text{Equation 1}$$

The variable a denotes the extent of the imperfection, while 'M_1' represents an experiential coefficient for the C/S area of the rail/weld head. Factor '1.12' was defined for the influence of the open surface or the proximity of the defect to the rail's operational surface. 'E(k)' indicates the elliptical integral of the second order, and it is a function dependent on the aspect ratio of the ellipse. It can be determined through the following method:

$$E(k) = \int_0^{\pi/2} \sqrt{1 - k^2 sin^2\theta}\ d\theta \qquad \text{Equation 2}$$

Where $k = \sqrt{1 - \left(\frac{a}{c}\right)^2}$

The stress term σ is the sum of three parts:

$$\sigma = \sigma_R + \sigma_N + M_G \sigma_B$$

The equation presented involves various stress components, namely the residual stress (σ_R), normal stress under axial force (σ_N), bending stress because of applied vertical force (σ_B), and an empirical factor (M_G) that serves to consider the stress gradient resulting from rail bending.

Methodology

In this study, a flanged wheel with a diameter of 1150 mm is modelled in ANSYS with its Space-claim module. The parent rails used in the simulation were UIC60, and a weld having 35 mm length

and sides extruded of 1 mm like a real un-grinded side of AT weld is integrated following Indian railways, shown in Figure 4. The wheel-rail assembly is exported to ANSYS structural workbench

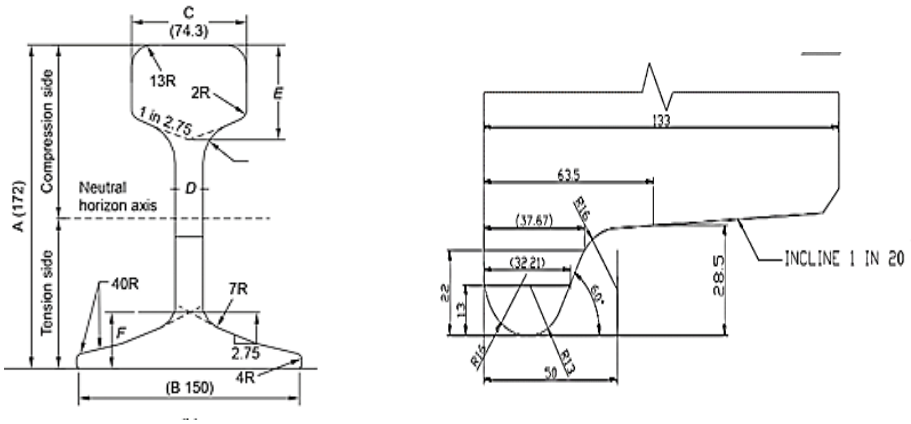

from space-claim for material assignment of parent rail, weldment, and wheel, as presented in Tables 1, 2 [19], and Table 3 presents the material composition used for UIC60 rail for Indian Railways.

Figure 4 Geometric features and final CAD view of assembly for simulation.

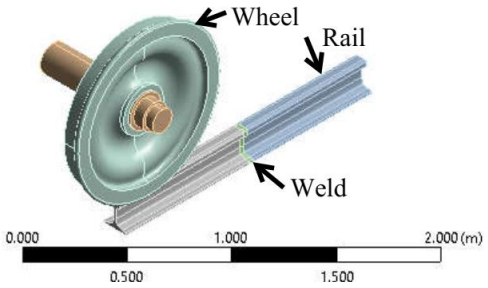

Table 1 Material properties of the weldment.

Property Name (Mechanical)	Poison Ratio	Young's Modulus (GPa)	UTS (MPa)	Yield Strength (MPa)	% Reduction area	% Elongation
Value	0.3	207 GPa	996.7 MPa	675.7 MPa	4.22	3.09

Table 2 CAD assembly's mechanical properties.

Part	Modulus E (GPa)	Plasticity Modulus	Yield Stress (MPa)	Poison Ratio
Rail	206.9	22.7	483	0.295
Wheel	205	22.7	640	0.3
Axle	205	-	-	0.3

Table 3 UIC60 rail steel composition.

Grade	880
Carbon	0.6-0.8
Manganese	0.8-1.3
Silicon	1.3-0.5
Sulphur (max.)	0.04

Phosphorous (max.)	0.04
Aluminium (max.)	0.02
Liquid H_2	3

The tangential tractions are represented as a function of the normal contact loads using friction coefficients. The failure to update contact conditions during plastic deformation in contact may lead to inadequate consideration of reducing effective contact loads, thereby limiting this method. The Hertzian theory exhibits limitations in accurately representing the physical contact between a rail and a wheel, presenting an additional challenge. The present investigation aims to address the complete contact conditions (contact interface linking the rail with the wheel) by using boundary conditions with FEM simulation. The mesh is employed to wheel rail assembly. The wheel is subjected to loading and rotation in the longitudinal rail direction. Figure 4 illustrates the complete FEM model. The assembly was discretized in eight nodes and brick-type elements with 11,418 and 12,516 pieces for rail and wheel, respectively having high mesh density and characterized by the elastic-plastic material's attributes.

The UIC rail weighing 60 kg was used to simulate on 200 mm rail track section with weld. Each FEM model comprises distinct inner and outer separated portions. Tables 1 and 2 show the assigned mechanical properties employed in the model for analysis are mentioned. The wheel diameter has a conical surface of 860 mm. The rail model's interior component measures 30 mm in width, 100 mm in length, and 15 mm in depth. The stress level in this location is relatively mild, and the surrounding areas exhibit characteristics of an elastic environment. Linear-elastic materials are employed to represent the volumes present within these components. The Multi-Point Constraint (MPC) technique addresses the discrepancy between the surface element patterns of adjacent inner and outer components.

Elastic straight beam elements represent the axle, allowing for freedom in rotation along three global directions. The wheel is affixed with rigid beam components that possess a diameter of 0.1 mm, rendering their presence negligible. The inflexible beam elements include identical elastic modulus and diameter compared to the axle. The axle is under a vertical wheel load of a magnitude of 69 kN, provided with a rotation of approximately 7^0 in the longitudinal direction, considered pure rolling. The frictional coefficient between the contact is set as 0.3. A plastic shakedown for material response is at contact, which can be demonstrated in the stress-strain curve. The criteria proposed by Jiang and Sehitoglu [20] for these responses were observed to be applicable in RCF conditions, as evidenced by a comparative assessment. This criterion calculates the fatigue life and the orientation of cracks. These criteria were implemented on each element with the load on the CAD model. The plane having a crack, commonly called a critical plane for fracture initiation, was

estimated based on the results obtained from the FEM simulation [21]. This critical plane is defined as the plane where the accumulation of the highest level of damage occurs, specifically concerning the fatigue parameter FP_{max}, during every instance of wheel passage. The model suggests that plastic deformation within the contact region results in the alteration of contact conditions, thereby enabling the consideration of decreased effective contact loads. The lower surface nodes of the rail are constrained solely to the vertical orientation, with an inclination of 1.43 degrees within the rail.

Furthermore, the rail model's cross-sections are subjected to two distinct constraints. The first constraint for model I: All nodes having degrees of freedom at both C/S are fixed. The secondary constraint for model II: All node's degrees of freedom are immobilized on one of the cross-section's points, whereas it remains unrestricted at the other end. It is believed that the current situation lies within the constraints of limitations that the proposed model is simulated under a limited number of wheel passages. Second the study only considers the effects of RCF cracks and does not consider other types of defects or damage mechanisms that can affect performance. The axle model's node is secured on the horizontal plane along its longitudinal plane of symmetry.

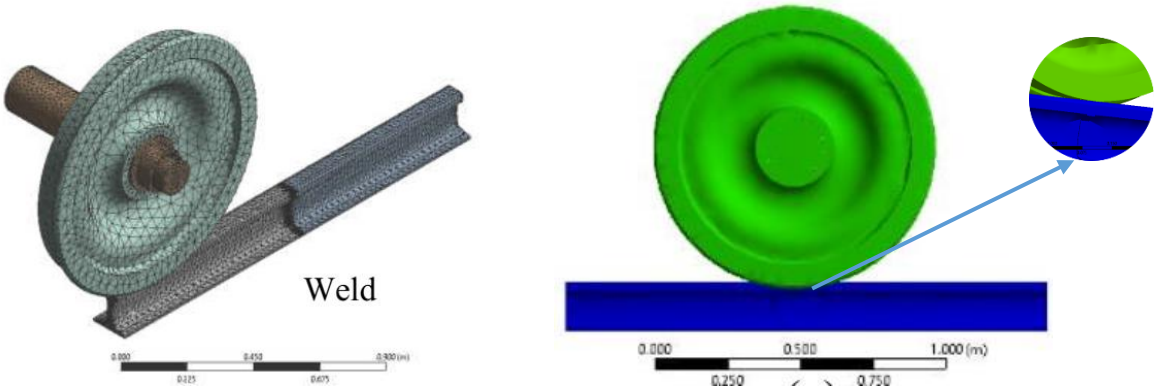

(a)Meshed assembly (b) Simulation view

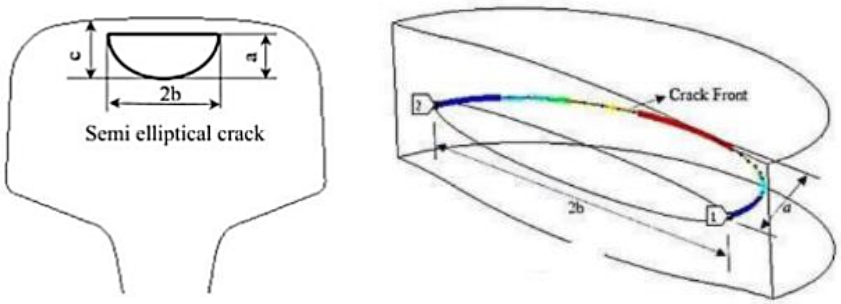

(c) Crack in ANSYS

Figure 5 Fine mesh model assembly with simulation view and semi-elliptical crack in ANSYS.

Crack Initiation as Squats

Fatigue cracks are described using a three-phase model encompassing crack initiation, growth, and fatigue life. Three stages of crack initiation are the initiation of a crack on the surface due to shear stress, followed by the transient growth of the crack and finally, the growth of the crack under the influence of both tensile and shear stresses. The emergence of cracks at rolling contact surfaces is attributed to the damage accumulation from combined rolling and sliding contact loading. It can be inferred that crack initiation occurred in the present investigation after-the-completion of Stage I. During analysis, a semi-elliptical shape crack was introduced onto the surface of the weld for simulation. The crack's geometry is depicted in Figure 5(c).

Results

Ten wheel passages were conducted on the provided models and estimations were made regarding the crack angles and cycle counts for initiating cracks. The simulation procedure involves four steps: firstly, placing the wheel onto the weld head and applying the load wheel axle; secondly, rotating the wheel with a constant load of 69 kN on the longitudinal surface; thirdly, removing the load after rotation angle of 7^0 and then separating wheel from the rail surface; and finally, returning the wheel to its initial position. The illustration presented in Figure 6(a) portrays Von Mises's stress in the railhead that occurs when a tenth wheel passes over it, as modelled.

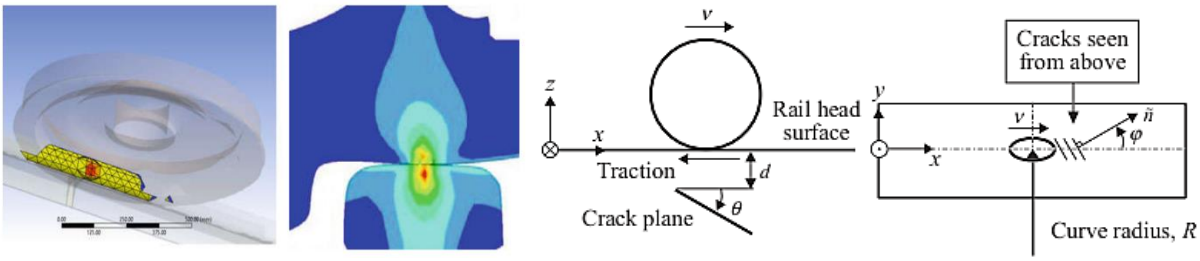

(a) (b)

Figure 6 (a) Von-Mises Stress for weld surface (b) Angles shown to start a crack on their crack plane (v indicates that object is rolling in that specific direction)

The depicted image portrays the spatial relationship between the contact portion and lengthwise alignment of the fusion joint. The angles in Figure 6(b) determine the crack plane direction, with the variable "v" representing the wheel's rolling direction. The angle θ represents the inclination w.r.t. the crack plane and x-axis, while angle ϕ denotes the azimuthal angle w.r.t the normal to crack plane and x-axis, as viewed from a top-down perspective. Figure 8 (a) is a process flow view of model assembly and crack orientation under simulation.

After completing 10 wheel passages on the weld, the parameter of maximum damage, represented as FP_{max}, and the cycle count leading to fracture initiation are calculated for models I and II. The

crack initiation cycle count was done using reference [20,21] concerning the maximum damage FP_{max}. Figure 8(b) exhibits the variations of FP_{max} that arise due to the passage of the wheel. Following ten wheel crossings, the FP_{max} values for models I and II converged to 0.22 and 0.25, respectively. Table 3 presents a summary of the angles of the crack planes.

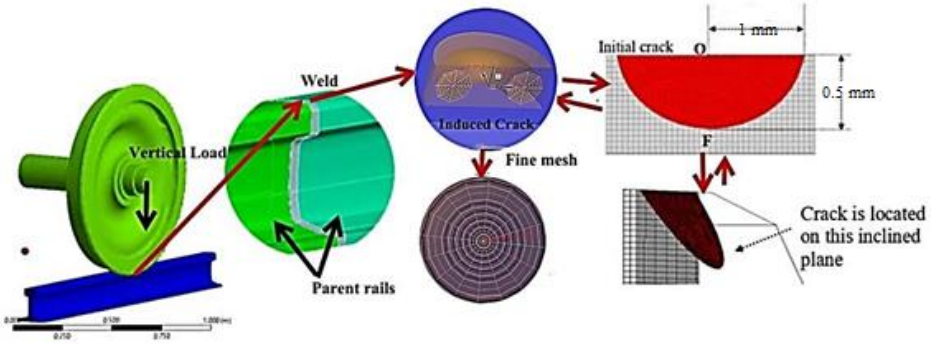

(a)

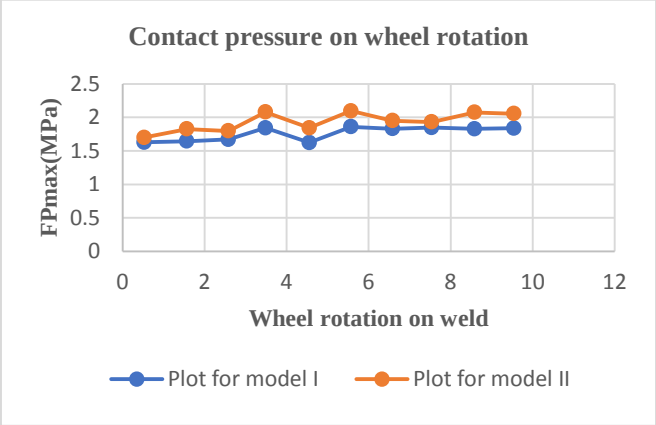

(b)

Figure 8 (a) Crack initiation simulation in ANSYS (b)Variations of FP_{max} referring No of the passage of wheel

Table 3 Results show FP_{max} and No. of Cycles for crack angles

Results for both models	Model	
	Model I	Model II
θ (deg)	0	25
Φ (deg)	0	10
Max. Damage FPmax(MPa)	0.223	0.252
N_f (Total cycle count for crack initiation)	7.46×10^6	3.86×10^6

RCF of the roller's surface defect and life were computed through microscopic observations for small fracture initiation and propagation, along with experiments performed on a two-disc wear machine with a fixed diameter of 60 mm for both specimens. The maximum contact pressures ranged from 580 to 1360 MPa, and the rotation speed was 400 rounds per minute [22]. The current study estimates that the P_{max} (maximum pressure) generated at the contact region using the Hertz hypothesis is 1092 MPa. The research findings indicate that at the point of crack initiation, defined

as fracture length of 0.5 mm on the curve of maximum contact pressure P_0=1100 MPa (Figure 9), projected along the final slope, resulting in approximately 2×10^6 cycles.

The present investigation reveals that the numerical prediction estimates the initiation of 0.5 mm-long cracks; the cycle counts are: for Model I =7.46×10^6 cycles and Model II=3.86×10^6 cycles. During the conclusive phase of the rolling contact experiments conducted by Liu et al. [25], the cracks exhibit propagation along the circumferential orientation of the roller. The crack plane direction is projected as the angle θ in the present investigation. Here, the crack plane direction is taken as for $\theta_{\text{model I}}$ equals 0° and for $\theta_{\text{model II}}$ equals 25°.

Discussion

The present study evaluated RCF fractures during rail wheel contact, focusing on the weldment section. The present investigation involves the loading and rotation of the wheel in the longitudinal direction of the rail. As per the proposed model, plastic deformation in the contact region leads to variation in the contact area, thereby enabling the consideration of a reduction in effective contact loads. The computational process is highly time-intensive, as evidenced by the FEM analysis of a single wheel passage utilizing ANSYS and a 2.4 GHz clock speed i7 processor, which requires approximately 44 hours to finalize. The execution of case studies can be facilitated by modifying loading conditions, wheel-rail geometry, and material properties. The present study primarily addresses squats occurring in the railhead section of the weldment.

Ringsberg [1] conducted a computational analysis to forecast the lifespan of crack initiation in the railhead's upper region. The proposed methodology depends on contact area pressure and creep stress generated on the contact interface on the line of symmetry of the rail model's upper surface and the propagation of these forces in the rolling direction. The study determined the longitudinal and transverse friction coefficients to be 0.25 and 0.31, respectively, while the wheel load was measured at 59 kN. Moreover, the yielding stress of 400.1 MPa was observed in the present model, which was less than yield stress of the weldment given in table 2. The fatigue performance of 16 wheel passages was evaluated through FEM simulations. The result revealed that the contact area between the wheel and rail exhibited a plastic shakedown response under a boundary condition. The crack formation was estimated to commence after 6.6106 wheel passes in the simulation. Regrettably, the literature failed to specify the calculated angle of the crack plane. The agreement is deemed satisfactory given the non-uniformity of the values on fatigue property of used material and contact pressure (maximum) in the present study and Ringsberg's numerical conditions. The available literature lacks sufficient experimental data sources to corroborate the numerical findings of the research. Li et al. [20] investigated the behaviour of short cracks in the medium carbon steel

roller at contact (having the material composition as 0.42%Si,0.43%C,0.023%P,0.026%S,0.52%Mn) under varying contact load and pure rolling criteria. The literature suggests these values are comparable to the present research [1,2]. The fatigue properties, specifically the fatigue strength coefficient (σ'_f), fatigue ductility coefficient (ε'_f), fatigue strength exponent (b), and fatigue ductility exponent (c), have not been defined adequately in literature [21]. Regrettably, Liu's research [21] lacks any findings regarding ϕ. There exist variations in the size of the considered samples. Additionally, the material's mechanical properties to fatigue and maximum pressure at the contact patch are not identical to the present numerical and laboratory test configurations. Thus, it is imperative to consider the influence of size, and the agreement may be acceptable.

Field observations indicate that cracks begin at regular intervals of a few hundred meters in the longitudinal orientation of the rail weld assembly. This event occurred after approximately 2×10^7 wheel cycles, with an axle load = 80 kN, $Radius_{wheel}$ = 910 mm, and UIC60 rail [23]. The current simulation study result suggests an earlier crack beginning at 3.86×10^6 and 7.46×10^6 cycles, considering identical contact positions in real-time. Values observed in contact between the wheel and rail demonstrate variability with each successive wheel passage, leading to a relatively reduced level of damage. A crack must have a specific length to be apparent to the naked eye on welding surfaces. This study employs fatigue cracks considering squats on the rail weld head. The model mentioned above also exhibits the capability of shelling within the wheel tread.

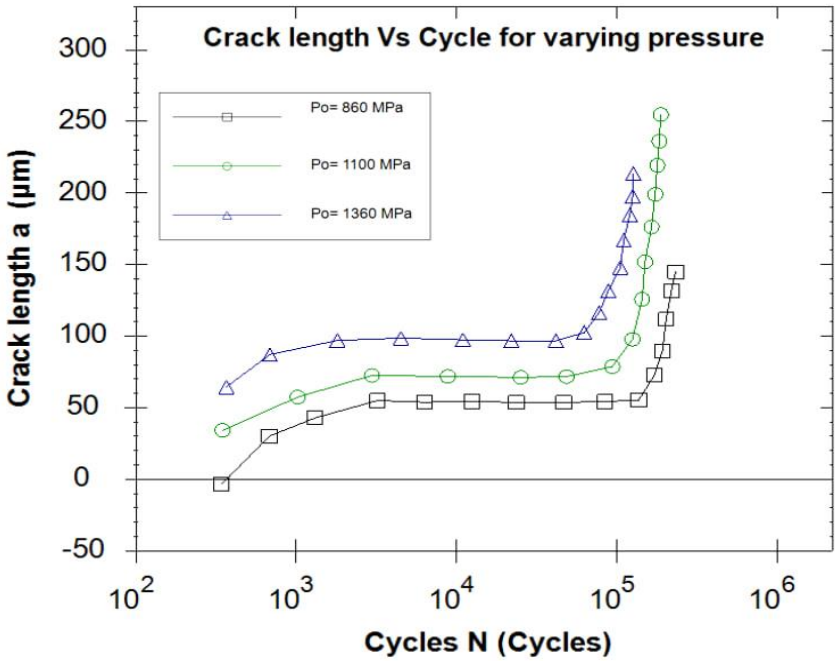

Figure 9: Graph between short crack length Vs. Rotation cycle for different max. contact pressure P_0.

Conclusions

The paper discusses the problem of RCF cracks on rail wheels and weld surfaces in the railway industry. The result predict the cycle required to initiate crack growth with fatigue damage parameter for rail weld given by maximum contact pressure. The present study result suggests an earlier crack beginning at 3.86×10^6 and 7.46×10^6 cycles, considering identical contact positions in real-time.

The proposed model can be used to predict the fatigue life of rails and optimize maintenance schedules to reduce the risk of catastrophic failures. The model can also be used to design new rail materials and geometries more resistant to RCF cracks.

- **Future work**

A more accurate model could be developed in future work to predict the crack growth rate and fatigue life of rails. This can be achieved by incorporating more complex material models and considering the effects of residual stresses and environmental factors.

- **Limitation**

The paper has a few limitations, such as:

1. Generally, the simulation is highly non-linear for multibody system model and is difficult to assess in a real-time environment.
2. The rail weld model was assumed, made of an Alumino-Thermite process. This may not be true in all situations.
3. The simulation excluded the effect of environmental factors such as temperature and humidity on the occurrence of squat cracks.
4. The model considered the only standard Indian rail wheel and UIC 60 rails with squat cracks in the present study.

References

[1] Ringsberg, J. W., Bjarnehed, H., Johansson, A., & Josefson, B. L. (2000). Rolling contact fatigue of rails—finite element modelling of residual stresses, strains and crack initiation. Proceedings of the Institution of Mechanical Engineers, Part F: Journal of Rail and Rapid Transit, 214(1), 7-19.

[2] Ringsberg, J. W., Life prediction of rolling contact fatigue crack initiation, International Journal of Fatigue, Vol. 23, No. 7 (2001), pp. 575-586.

[3] Bogdański, S., & Brown, M. W. (2002). Modelling the three-dimensional behaviour of shallow rolling contact fatigue cracks in rails. Wear, 253(1-2), 17-25.

[4] Dubourg, M. C., & Lamacq, V. (2002). A predictive rolling contact fatigue crack growth model: onset of branching, direction, and growth—role of dry and lubricated conditions on crack patterns. J. Trib., 124(4), 680-688.

[5] Shitara, H., Terashita, Y., Tatasumi, M., & Fukada, Y. (2003). Nondestructive testing and evaluation methods for rail welds in Japan. Quarterly Report of RTRI, 44(2), 53-58.

[6] Terashita, Y., & Tatsumi, M. (2003). Analysis of damaged rail weld. Quarterly Report of RTRI, 44(2), 59-64.

[7] Böhmer, A., & Klimpel, T. (2002). Plastic deformation of corrugated rails—a numerical approach using material data of rail steel. Wear, 253(1-2), 150-161.

[8] Mutton, P. J., & Alvarez, E. F. (2004). Failure modes in aluminothermic rail welds under high axle load conditions. Engineering Failure Analysis, 11(2), 151-166.

[9] Hiensch, M., Nielsen, J. C., & Verheijen, E. (2002). Rail corrugation in The Netherlands—measurements and simulations. Wear, 253(1-2), 140-149.

[10] Li, Z., Zhao, X., Esveld, C., & Dollevoet, R. (2006). Causes of squats: correlation analysis and numerical modeling. In 7th Int. Conf. on Contact Mechanics and Wear of Rail/Wheel Systems (pp. 439-446). Institute of Materials Engineering Australasia Ltd.

[11] Li, Z., Zhao, X., Esveld, C., & Dollevoet, R. P. B. J. (2007, June). Rail stresses, strains and fatigue under dynamic wheel-rail interaction. Proceedings International Heavy Haul Conference, Specialist Technical Session, 11-13 June 2007, Kiruna, Sweden (pp. 389-396). Lulea University of Technology Press.

[12] Hearle, A. D., & Johnson, K. L. (1985). Mode II stress intensity factors for a crack parallel to the surface of an elastic half-space subjected to a moving point load. Journal of the Mechanics and Physics of Solids, 33(1), 61-81.

[13] Keer, L. M., Farris, T. M., & Steele, R. K. (1986). On some aspects of fatigue crack growth in rails induced by wheel/rail contact loading. Proceedings of the 2nd International Symposium on contact Mechanics and Wear of Wheel/Rail Systems, URI, University of Waterloo Press.

[14] Ishida, M., Akama, M., Kashiwaya, K., & Kapoor, A. (2003). The current status of theory and practice on rail integrity in Japanese railways—rolling contact fatigue and corrugations. Fatigue & Fracture of Engineering Materials & Structures, 26(10), 909-919.

[15] Deroche, R. Y., et al. (1992). RCF cracks on SNCF conventional tracks. In Rail quality and maintenance for modern railway operation, J. J. Kalker, et al. (Eds.). Alphen aan den Rijn, the Netherlands: Kluwer Academic Publishers.

[16] Kondo, K., Yoroizaka, K., & Sato, Y. (1996). Cause, increase, diagnosis, countermeasures and elimination of Shinkansen shelling. Wear, 191(1-2), 199-203.

[17] Li, Z., Zhao, X., Esveld, C., Dollevoet, R., & Molodova, M. (2008). An investigation into the causes of squats—Correlation analysis and numerical modeling. Wear, 265(9-10), 1349-1355.

[18] David Y. Jeong, Correlations Between Rail Defect Growth Data and Engineering Analyses, Part I: Laboratory Tests U.S. Department of Transportation Research and Special Programs administration Volpe National Transportation Systems Center Cambridge, Massachusetts 02142.

[19] Wang, Y. Q., Zhou, H., Shi, Y. J., & Feng, B. R. (2012). Mechanical properties and fracture toughness of rail steels and thermite welds at low temperature. International Journal of Minerals, Metallurgy, and Materials, 19(5), 409-420.

[20] Jiang, Y., & Sehitoglu, H. (1999). A model for rolling contact failure. Wear, 224(1), 38-49.

[21] Akama, M. (2007). Development of finite element model for analysis of rolling contact fatigue cracks in wheel/rail systems. Quarterly Report of RTRI, 48(1), 8-14.

[22] Li, Y., Kang, G., Wang, C., Dou, P., & Wang, J. (2006). Vertical short-crack behavior and its application in rolling contact fatigue. International journal of fatigue, 28(7), 804-811.

[23] National Research Institute for Metals, NRIM Fatigue Data Sheet, No.2, Data Sheets on Fatigue Properties of S35C (0.35C) Steel for Machine Structural Use, 1978.

[24] Zhang, S. Y., Spiryagin, M., Ding, H. H., Wu, Q., Guo, J., Liu, Q. Y., & Wang, W. J. (2022). Rail rolling contact fatigue formation and evolution with surface defects. International Journal of Fatigue, 158, 106762.

[25] Nejad, R. M., Liu, Z., Ma, W., & Berto, F. (2021). Reliability analysis of fatigue crack growth for rail steel under variable amplitude service loading conditions and wear, International Journal of Fatigue, 152, 106450.